A Dual-Transport Model of Moisture Diffusion in PV Encapsulants for Finite-Element Simulations

Stefan Mitterhofer, Chiara Barretta, Luis F. Castillon, Gernot Oreski, Marko Topič, and Marko Jankovec

***Abstract*—A better understanding of moisture ingress in photovoltaic modules is crucial for better predictions of their long-term behavior in the field. Current calculations and simulations of moisture uptake in photovoltaic modules are based on the Fickian diffusion model in a homogeneous material. In this article, *in situ* humidity measurements in four different encapsulants exposed to transient humidity conditions are compared with Fickian simulations. It is found that the model cannot accurately describe the measured moisture ingress and egress curves. Thus, a new model for finite-element simulations based on two transport mechanisms is applied. The mesh is split into two regions, where channels with a high diffusion coefficient lead through a bulk with a low diffusion coefficient. The diffusion in both regions as well as the flow between them is simulated as Fickian. The new model is able to predict the measured ingress and egress curves more accurately than the Fickian model in all four encapsulants. The same simulation parameters can accurately describe ingress for various relative humidity values between 20% and 80%, as well as egress from 40% to 20%. This allows further prediction of moisture ingress after the measurement of a single ingress curve and a corresponding parameter optimization. However, a nonlinearity of the diffusion during egress at higher moisture values in the encapsulants is found.**

***Index Terms*—Finite-element simulations, moisture ingress, photovoltaics (PVs), polymers.**

I. Introduction

PHOTOVOLTAIC (PV) modules installed in the field experience a wide variety of climatic stresses. Moisture is one such factor affecting their degradation, in forms of relative humidity (RH) in the air, dew, and precipitation. It can ingress into the polymers used as encapsulants and backsheets, influencing various degradation modes of modules mounted in the field. Examples include yellowing and browning of the encapsulant, delamination, corrosion and potential-induced shunting [1]–[5]. The consequences can be severe power losses and safety issues [3]. Thus, understanding moisture ingress into PV modules and different materials used in their production is crucial to ensure a long lifetime and operation in the field.

Simulations and calculations of moisture ingress in PV modules and encapsulants are based on the Fickian diffusion model [6]–[15]. The material is homogeneous and described by a single diffusion coefficient D. It shows a temperature (T) dependence according to the Arrhenius law, but is independent of the moisture concentration. However, moisture ingress in polymers is a complex topic. It is influenced by many material parameters, including the polymer network structure [16], polarity [16], microvoids in the material [17], free volume [18], crystallinity [19], and cross-linking degree [20], to name a few. Mechanical stress and strain further affect the ingress [21]. Diffusion along interfaces between materials and between different phases in the material is different from diffusion in the bulk [22]. The material can change its properties while aging, changing the ingress between sorption, desorption, and resorption [23]. Furthermore, polymers are a large group of materials and measured ingress curves can vary a lot from each other. Theories resulting in more accurate simulations or calculations for some polymers may not yield similar improvements for others, or may not be applicable due to a different polymer structure.

Thus, it is no surprise that the simple Fickian model applied to a homogeneous material shows limited accuracy in predicting the measured ingress curves in PV encapsulants, for example, ethylene vinyl acetate (EVA), thermoplastic olefins (TPO), polyolefin elastomers (POE), and ionomers [24].

Many non-Fickian models have already been applied for a more accurate description of moisture ingress measurements in other polymers. A common approach is to include two main mechanisms driving the diffusion process. There are many theories about the nature of these two mechanisms, varying for different materials. Some theories are based on the heterogeneity of the polymer, having two different values of D, based on polarity [25] or density [26]. In others, two states of water in the polymer are presumed. Water is ingressing either as single molecules or as molecule clusters [27]. Other theories describe two different types of interaction between water and polymer. Water can be bound with single or multiple hydrogen bonds in hydrophilic polymers [28]. Another theory describes the sorption of water either in the free volume or in hydrogen-bonded clusters in the polymer structure [29]. One theory presumes the material relaxation after hygroscopic swelling driving a second, slower diffusion process [30].

Manuscript received July 18, 2019; revised October 18, 2019; accepted November 19, 2019. Date of publication December 3, 2019; date of current version December 23, 2019. This work was supported in part by the European Union's Horizon 2020 research and innovation program in the framework of the project "SolarTrain" under the Marie Sklodowska-Curie GA 721452—H2020-MSCA-ITN-2016 and in part by Slovenian Research Agency under the research program P2-0197. *(Corresponding author: Stefan Mitterhofer.)*

S. Mitterhofer, M. Topič, and M. Jankovec are with the Faculty of Electrical Engineering, University of Ljubljana, 1000 Ljubljana, Slovenia (e-mail: stefan.mitterhofer@fe.uni-lj.si; marko.topic@fe.uni-lj.si; marko.jankovec@fe.uni-lj.si).

C. Barretta, L. F. Castillon, and G. Oreski are with the Polymer Competence Center Leoben, 8700 Leoben, Austria (e-mail: chiara.barretta@pccl.at; luis.castillon@pccl.at; gernot.oreski@pccl.at).

Color versions of one or more of the figures in this article are available online at http://ieeexplore.ieee.org.

Digital Object Identifier 10.1109/JPHOTOV.2019.2955182

Fig. 1. Miniature sensor (left) and sensor strip in the encapsulant (right).

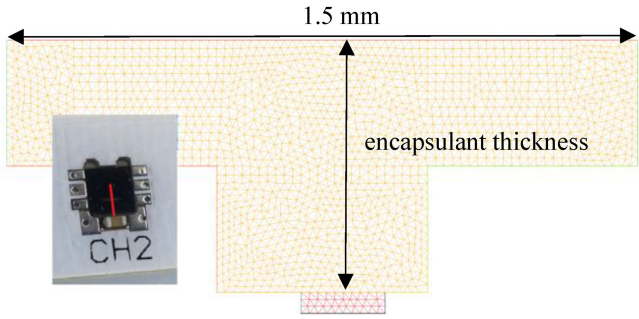

Fig. 2. Mesh used for Fickian simulations. The small picture shows an encapsulated *T* and RH sensor. The geometry for the boundaries of the mesh is taken from the two-dimensional cross section along the red line. The red area at the bottom of the mesh represents a polymer used by the sensor for its capacitive measurements. The measured encapsulant thicknesses are given in Table I.

TABLE I
MEASURED ENCAPSULANT THICKNESS ABOVE THE THREE SENSORS

Thickness above:	EVA	TPO	POE	ionomer
sensor 1 (μm)	570	n/a	480	690
sensor 2 (μm)	645	630	570	525
sensor 3 (μm)	615	600	630	525

Different approaches were taken to implement non-Fickian models in simulations and calculations to predict moisture ingress on a macroscopic scale. One approach added sources and sinks for moisture in the material, defined two states of water and mathematical probabilities to change from one to the other, creating a system of two coupled differential equations [31]. Other approaches include the development of analytical models for simple geometries [26], or decoupling both processes, simulating them independently and sum up the results [32]. Recent work has tried to combine molecular simulations and calculations of flow in nanochannels with macroscopic diffusion through membranes [33]. However, a model and fitting theory for PV encapsulants is still missing in literature.

In this article, we propose and evaluate such a model based on an inhomogeneous morphology of the material. First, the used measurement setup based on miniature T and RH sensors is presented. Then, simulations based on the Fickian diffusion model in a homogeneous material are described. Their results are analyzed and compared with the measurements, showing the shortcomings of the model and the need for a new, more accurate model. The basic ideas behind the proposed new model are described. The model is based on channels running through the bulk of the material and driving the diffusion. The parameters of the simulation, their impact on the results, and the flow of moisture in the model are analyzed. The results are compared with the measurements of four different polymers. In the end, a discussion compares the model with possible physical explanations taken from the literature of other models based on two moisture transport mechanisms.

II. MEASUREMENT SETUP

Printed circuit board strips containing miniature T and RH sensors [34] are encapsulated between two layers of PV encapsulants, as shown in Fig. 1 [35]. One strip contains three sensors inside the polymer and one sensor outside to measure T and RH in the air. The analyzed materials are commercially available EVA, POE, TPO, and ionomer. The strips are connected to custom readout electronics. The setup is controlled by a custom software written in LabVIEW. Measurements are taken every 60 s. A more in-depth description of the setup is published elsewhere [34], [35].

Ingress and egress between 20% and 40% RH, 20% and 60% RH, as well as 20% and 80% RH, at 50 °C are measured inside a climatic chamber.

III. FICKIAN SIMULATIONS

In this section, the simulations based on the Fickian model in a homogeneous material are described. It is the current state of the art for moisture transport simulations in PV encapsulants. The FreeFEM++ software is used in the simulations with the FreeFEM++−cs development environment [36].

A. Mesh Creation

The mesh used in the simulations is shown in Fig. 2. The thickness of the encapsulants above the sensors is measured optically. The sample is placed under a microscope. The focus is set to the active area of a sensor. Then, it is changed to the surface of the encapsulant. This process is repeated several times in both directions. The thickness is calculated from the so-obtained optical depth and the refractive index of the materials. The latter is rounded to 1.5, which is a reasonable approximation for common PV encapsulants. The results are shown in Table I. Depending on the roughness of the surface and small possible indentations on a micrometer scale, the accuracy of the thickness measurement is estimated to be $\pm 10\%$ of the respective value.

The thicknesses are all larger than the datasheet values of the encapsulants. This is caused by the indentation of the sensor containing the sensor's active area is. During lamination, it is filled with encapsulant, adding to the total thickness.

B. Differential Equation

Fick's second law of diffusion in two dimensions is the governing differential equation

$$\frac{\partial C}{\partial t} = \nabla \left(D \cdot \nabla C \right). \tag{1}$$

Here, C is the moisture concentration in the encapsulant. It is proportional to the measured RH at constant temperature.

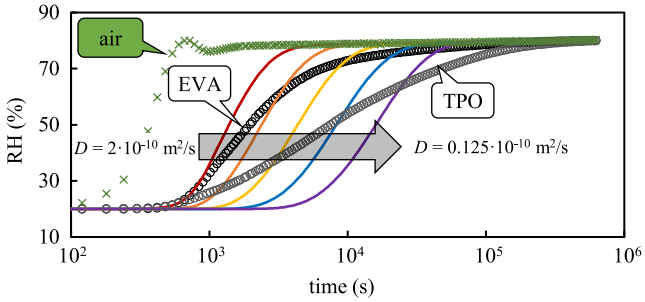

Fig. 3. Comparison between Fickian simulations (solid lines) with different D and measurement results (circles) of an EVA and a TPO. The value of D is halved each simulation, starting from $2 \cdot 10^{-10}$ m²/s.

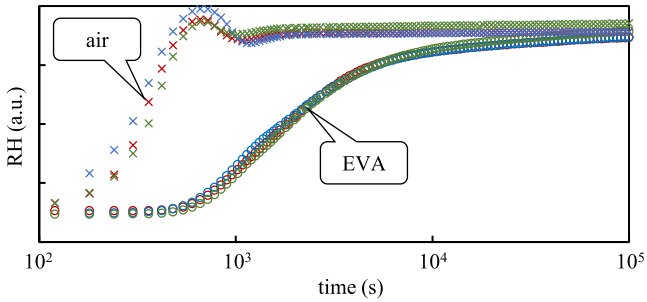

Fig. 4. Measured ingress curves of EVA from 20% to 40% (red), 60% (blue), and 80% RH (green), scaled to the same saturation value. The overlap of the curves shows that the moisture ingress dynamics into the material is not concentration-dependent.

The time is discretized into several time steps. They are set to coincide with the times at which measurements are taken. To keep the simulation times as low as possible, longer time steps during the later stages of the ingress are taken. The solution at time-step m is obtained with the Crank–Nicolson method [37]. The resulting weak form of (1)

$$0 = \int_\Omega \left(C_m v + \frac{1}{2} D \cdot \delta t \cdot \nabla C_m \cdot \nabla v \right) d\Omega - \int_\Omega \left(C_{m-1} v - \frac{1}{2} D \cdot \delta t \cdot \nabla C_{m-1} \cdot \nabla v \right) d\Omega. \quad (2)$$

Here, v is any test function $v \epsilon H^1(\Omega)$, δt the duration of the time-step between m and $m-1$.

C. Boundary Conditions

A Dirichlet boundary condition is set along the interface of the material to the air. It is the average of the RH measured in the air at the beginning and the end of the time-step. The flow across all other outer boundaries is set to 0.

D. Simulation Results of Homogeneous Encapsulants

The results of the measured *RH* in the encapsulants compared with the Fickian simulations using various values of D are shown in Fig. 3. Out of the four analyzed encapsulants, only two are presented for clarity. EVA yields the best fit between measurements and simulations, whereas TPO yields the worst fit.

Varying D only results in a translation of the simulated ingress curves in time. Their slope in the logarithmic time scale remains, indicating that the Fickian model with a single concentration-independent D cannot explain the results of the measurements.

A common approach to improve the Fickian model is the addition of a nonlinearity by the definition of a concentration-dependent D. A slower diffusion at high moisture concentrations would explain the discrepancies. To analyze this possibility, the ingress curves to 40%, to 60%, and to 80% are compared. However, the shapes of these ingress curves do not show any major differences, emphasizing that the absorbed amount of water does not change the moisture transport properties of these materials within the analyzed range, as shown in Fig. 4.

Another possibility is the impact of the sensor itself [35]. An undisclosed type of polymer is used in the sensor for capacitive measurements. It can take up a certain amount of water due to the moisture's solubility inside the material. It has no impact during measurements in the air, for which the sensors are built. However, this solubility can influence the results inside the encapsulant, where only limited amounts of moisture slowly diffuse to the sensor. This effect has been shown to slow down the apparent ingress [24]. While the results of the simulation are changed by considering it, it neither can account for the big discrepancies, nor explain the differences between the various encapsulants. A more in-depth analysis of this effect is given in Section V-A4.

Thus, we conclude that a new model is required for more accurate simulations of moisture diffusion in PV encapsulants.

IV. Dual-Transport Model Simulations

A. Basic Considerations

A new model including two different transport mechanisms is proposed to improve the accuracy of the simulations. The requirements set for this model are as follows.

1) It should build upon the previously used model.
2) It should be kept as simple as possible, with a low number of material parameters.
3) It should increase the accuracy of the simulations for all measured encapsulants using the same material parameter set.

To simulate these two mechanisms, the material is split into two regions, namely channels and bulk. This basic idea stems from previous attempts of combining flow in nanochannels with macroscopic flow in the literature [33]. Diffusion in both regions, as well as from one region to the other, is simulated with the Fickian diffusion equation (1). The diffusion coefficients are set such that diffusion is faster in the channels and slower in the bulk. The saturation moisture contents in bulk and channels are the same. The same boundary conditions as described in Section III-C are used. Thus, the only difference between the homogeneous Fickian model and the new model is the implementation of an inhomogeneous mesh with two diffusion coefficients. In the following, the "Fickian model" or "Fickian diffusion" denotes Fickian diffusion in a homogeneous material. For mesh creation

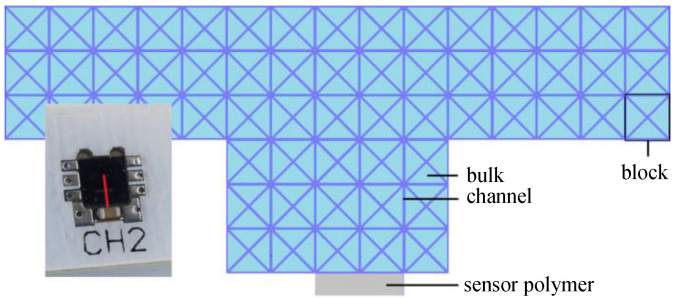

Fig. 5. Depiction of the channel configuration added to the material. The small picture shows an encapsulated *T* and RH sensor. The two-dimensional geometry is created along the cross section indicated by the red line. The additional gray area in the bottom is the polymer used in the sensor for the measurements.

TABLE II
SIMULATION PARAMETERS

Category	Parameter	Description
Geometry	S_C (%)	Share of channels in the material
	F_{geo}	Geometric factor
	H_{sens} (µm)	Height of the sensor polymer area
Mesh	Q_{mesh} (10·mm^{-1})	Mesh quality
Diffusion	D_B (m^2/s)	Diffusion coefficient bulk
	D_C (m^2/s)	Diffusion coefficient channel

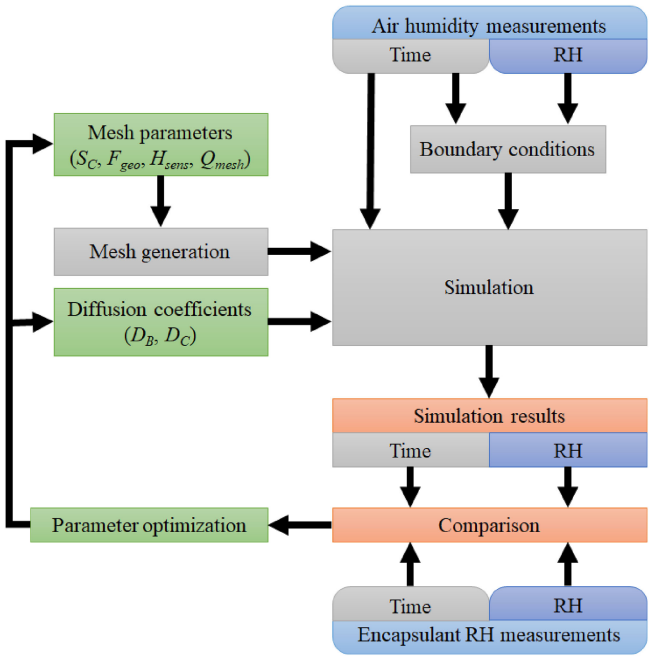

Fig. 6. Flowchart of the simulation and parameter optimization process.

and solving the differential equation, again the FreeFEM++ software with the FreeFEM++−cs development environment is used [36].

B. Simulations

The channels are implemented in four directions. This is a middle ground between a lower amount of directions, increasing the anisotropy caused by the geometry, and a higher amount, adding complexity to the model. An example of a model is shown in Fig. 5. In the simulations, the interface is considered as part of the bulk.

The simulation parameters are shown in Table II. Two parameters, S_C and F_{geo}, control the geometry of the channels in the material. S_C is the ratio between the total area of the channels and the total area of the entire mesh. The geometric factor F_{geo} determines the number of building blocks, the basic elements that are repeated, as shown in Fig. 5. Over the width of the entire mesh, the number of repeating blocks is $3{\cdot}F_{\text{geo}}$. Fig. 5 shows the model with $F_{\text{geo}} = 5$. The parameters F_{geo} and S_C together determine the width of the channels and the distance between them.

Parameter H_{sens} changes the size of the sensor polymer's area. If the diffusion coefficient in that area is very high, an increase of its size with a constant solubility of water in the material is equivalent to an increase of said solubility while keeping size constant in the simulations.

According to the datasheet, the RH response time of the sensor in the air is in range of seconds, thus moisture diffuses quickly in the sensing polymer. Therefore, we set its diffusion coefficient arbitrarily to 1 m^2/s. This value is many orders of magnitude larger than diffusion coefficients in the encapsulant, assuring diffusion through the sensor polymer itself does not influence the simulated ingress.

The parameter Q_{mesh} changes the quality of the mesh. Each boundary defined in the geometry is split into Q_{mesh} number of intervals every 0.1 mm to serve as base for the triangulation, i.e., the mesh creation. A higher value of Q_{mesh} results in a higher accuracy of the simulation, but increases the required time. The elements of the mesh are continuous piecewise quadratic.

C. Parameter Analysis and Optimization

First, the impact of the parameters on the simulation results is analyzed. Then, the parameters are manually optimized for the measured encapsulants. For this purpose, a rough approximation of these parameters is extracted from the previously obtained curves during the parameter analysis at first. Then, the trends of parameter variations and interaction between the parameters is analyzed in more depth close to this point. These trends are used to find a good fit between measurement and simulation, visually and with a minimized root-mean-squared error. Fig. 6 shows a flowchart of the optimization process.

V. RESULTS

A. Parameter Variation

The impact of the parameters on the simulation results is analyzed. The measurements of the sensor in the air during ingress from 20% to 80% RH are used as a time dependent boundary condition.

1) Variation of the Diffusion Coefficients: In this article, S_C is set to 10%, D_C to $5{\cdot}10^{-10}$ m^2/s, Q_{mesh} to 20, and H_{sens} to 50 μm. Parameter D_B is varied and kept lower than D_C, since our initial proposition was that bulk has lower diffusion rate

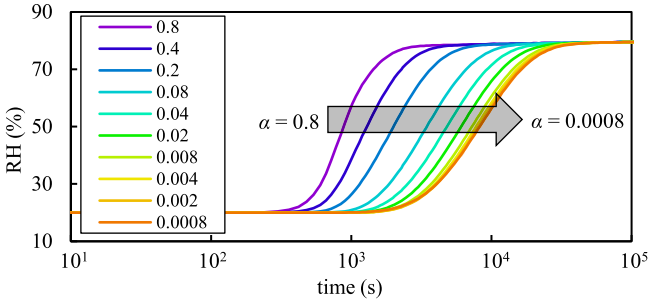

Fig. 7. Simulated ingress curves while reducing α and correspondingly the diffusion coefficient in the bulk D_B. $S_C = 10\%$, $D_C = 5 \cdot 10^{-10}$ m^2/s, $Q_{\mathrm{mesh}} = 20$, $H_{\mathrm{sens}} = 50$ μm.

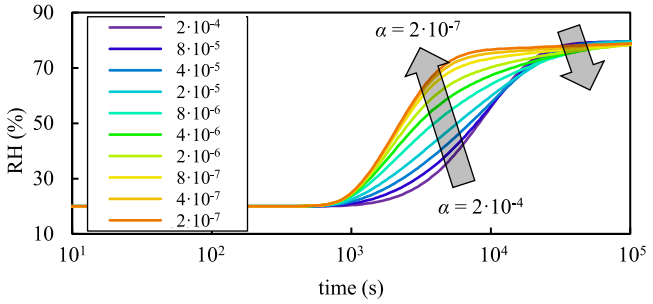

Fig. 8. Simulated ingress curves during further reduction of α and correspondingly D_B. $S_C = 10\%$, $D_C = 5 \cdot 10^{-10}$ m^2/s, $Q_{\mathrm{mesh}} = 20$, $H_{\mathrm{sens}} = 50$ μm.

than channels. We introduce parameter α as the ratio between D_B and D_C

$$D_B = \alpha \cdot D_C, \quad 0 \leq \alpha \leq 1. \tag{3}$$

When the value of D_B is in the same order of magnitude as $D_C (\alpha > 0.1)$, moisture is quickly absorbed from the channels into the bulk. The results are Fickian ingress curves, resembling the diffusion in a homogeneous material with a diffusion coefficient between D_C and D_B. Reducing α further, the results still resemble Fickian curves with only slight decrease of the slope, as shown in Fig. 7.

If α is reduced to a range between 10^{-3} and 10^{-4}, the interaction with the bulk becomes so slow that small amounts of moisture can reach the sensor through the channels without being absorbed in the bulk. This reverses the trend and causes a faster ingress shortly after the step change of the air humidity. Later, the moisture ingress becomes slower due to delayed bulk interaction, as shown in Fig. 8.

Reducing α further, the bulk becomes almost impermeable in the time scale the moisture takes to reach the sensor through the channels. The simulated ingress curves asymptotically approach a Fickian ingress curve at $\alpha = D_B = 0$.

In this way, a set of curves with different slopes can be obtained by only changing α and keeping all other parameters constant, with Fickian diffusion as limit at both limit cases: $\alpha = 0$ and $\alpha = 1$. Changing D_C causes this set of curves to move along the time axis, similar to a variation of D in the Fickian model.

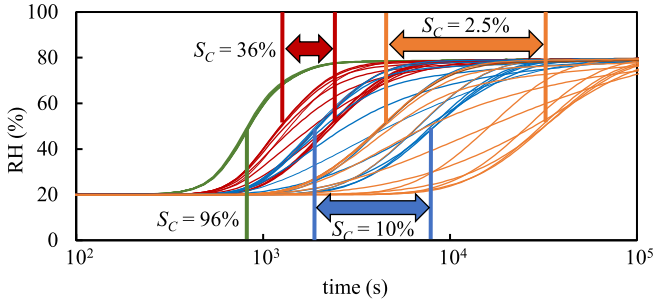

Fig. 9. Impact of varying the share of channels S_C on the sets of ingress curves. One set in this graph is obtained by keeping all parameters constant and only varying α between 0 and 0.2. The arrows denote the width of the respective set at 50% simulated RH. $D_C = 5 \cdot 10^{-10}$ m^2/s, $Q_{\mathrm{mesh}} = 20$, $H_{\mathrm{sens}} = 50$ μm.

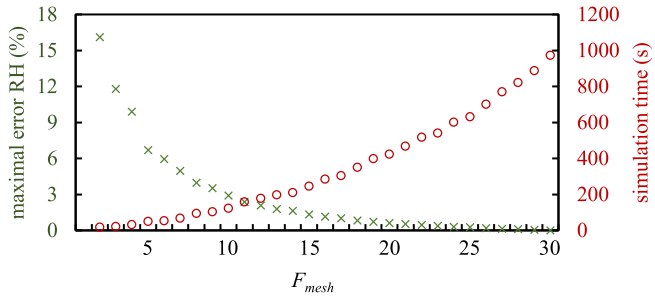

Fig. 10. Influence of the mesh quality on the maximal error (crosses, left axis) compared with the simulation with the finest used mesh. On the right axis, the simulation time is shown (circles). A very coarse mesh impacts the simulations by adding a large error, whereas a very fine mesh results in a very long time required.

2) Variation of the Share of the Channels: Increasing S_C raises the share of the channels in the entire mesh. Thus, diffusion through the channels becomes prevalent while the impact of the bulk becomes smaller. The simulated set of curves (obtained varying the ratio α) shifts to an earlier time by increasing S_C, while the range becomes narrower, finally breaking down to a single Fickian ingress curve at S_C approaching 100%, as shown in Fig. 9.

3) Variation of the Mesh Quality: Increasing the quality of the mesh by increasing the number of elements in the triangulation results in more accurate simulations at the cost of a longer required time, as shown in Fig. 10. In a homogenous geometry simulation problem, a coarse mesh is sufficient. However, the higher mesh quality is required in this case due to many material interfaces.

4) Variation of the Sensor Polymer: Increasing the size of the sensor polymer's area slows down the measured ingress curves primarily in the early stages of the diffusion, as shown in Fig. 11.

The properties of the sensor polymer, including the solubility of water inside it and correspondingly the parameter H_{sens} to simulate it, are unknown parameters for the simulations. The solubility does not change over time, shown by its repeatable measurements [38]. It can be set constant in all simulations.

5) Scale of the Geometry: Now that the influence of the parameters has been analyzed, a more detailed look on the scale of the geometry and the relation to the parameters is taken. For this purpose, a 100 $\times$ 100 μm area is analyzed. The number of

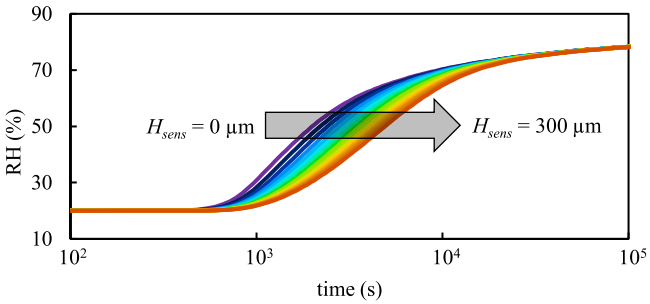

Fig. 11. Variation of the size of the sensor polymer. The parameter H_{sens} is changed linearly in steps of 20 μm.

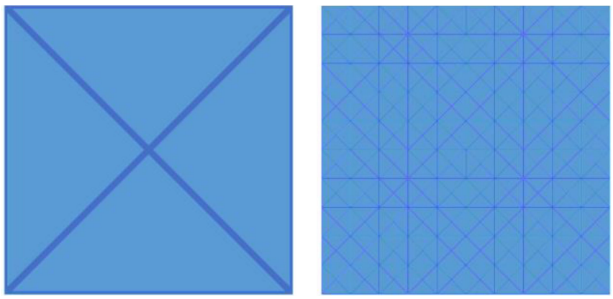

Fig. 12. Geometries used for an in-depth analysis of the impact of the scale of the geometry, consisting of 1^2 (left) to 10^2 (right) blocks.

blocks in one direction is increased from 1 to 10 in steps of 1 and their size reduced accordingly while S_C is constant at 10%, as shown in Fig. 12.

To calculate the moisture going through the entire stack, a 0.1-μm wide area with very high diffusion coefficient is added at the bottom. The output is the humidity in this area. The small width is chosen to minimize its solubility impact.

D_C is set constant at 10^{-1} m^2/s. Q_{mesh} is 20 times the number of blocks, changed to minimize the effects of a changing mesh quality in relation to the size of the triangles. For each case, α is optimized to minimize the average pointwise difference to the simulation with the highest resolution. The maximal absolute error while changing the number of blocks by one order of magnitude, as is the case in Fig. 12, is less than 1% RH.

If we keep the mesh quality Q_{mesh} constant, the simulated ingress curves deviate with an increasingly fine geometry. This limits the number of blocks, and accordingly F_{geo} in the simulations of the setup, in both directions. On one side, a very low value F_{geo} results in a larger error in the simulations. On the other side, a very high value F_{geo} requires an accordingly fine mesh not to result in a larger error, which significantly increases simulation time.

B. Visualization of Moisture Ingress in the Encapsulant

To visualize the pathway of moisture in the simulations, the moisture in the encapsulant is plotted at various times during an ingress simulation, as shown in Fig. 13. The parameters are taken from the optimization for the EVA measurements, as given in Table III.

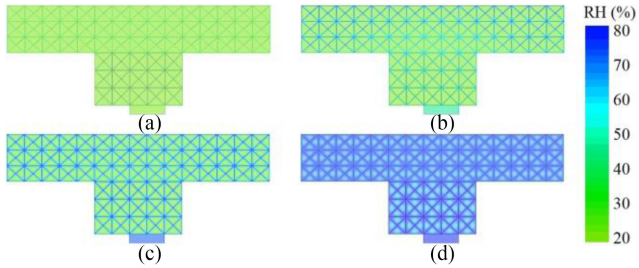

Fig. 13. Simulated moisture ingress after (a) 0 s, (b) 1600 s, (c) 9500 s, and (d) 104 700 s.

TABLE III
OPTIMIZED SIMULATION PARAMETERS AND MEASURED ENCAPSULANT THICKNESS ABOVE THE THREE SENSORS

Parameter	EVA	TPO	POE	ionomer
D_C (10^{-10} m^2/s)	4.5	7.5	10	0.72
α ($\cdot 10^{-6}$)	3.1	4	1.5	14
S_C (%)	10	2	2	4

This visualization shows how the model works with the parameters fitting the measured encapsulants. In the beginning, RH is at its initial value in the entire material, as shown in Fig. 13(a). As the air humidity changes, moisture starts diffusing into the channels, and through the channels to the sensor. During this time, the sensor shows a fast change in the measured humidity. Because the concentration gradient between channels and bulk is in general not large, and the diffusion coefficient in the bulk is much lower than in the channels, only very small amounts of water are absorbed into the bulk. This is shown in Fig. 13(b) and (c). As more water flows into the channels, the concentration gradient inside them gets smaller. Ingress into and through them is slowing down. However, at the same time the concentration gradient between bulk and channels becomes larger, driving a faster diffusion from the channels into the bulk. The longer this process continues, the closer also the bulk comes to its saturation level, which is equivalent to the humidity concentration in air. This is a very slow process compared to the initial diffusion because of the low diffusion coefficient of the bulk. This is shown in Fig. 13(c) and (d).

During this entire process, the channels are driving the diffusion through the sensor where the bulk acts as a hindrance to the Fickian diffusion process through these channels.

C. Parameter Optimization

The optimized simulation parameters are obtained by fitting the measured ingress curves at air humidity step change from 20% to 60% RH. Parameters $F_{\mathrm{geo}} = 5$, $Q_{\mathrm{mesh}} = 30$, and $H_{\mathrm{sens}} = 50$ μm are kept constant. The obtained fitting parameters are given in Table III.

After that, the same parameters are used to simulate moisture ingress at air humidity step changes from 20% to 40% and from 20% to 80%. In Fig. 14, only the comparison at the 20% to 40% RH air humidity step change are shown for clarity, although the fits are similarly good in all cases. This proves the

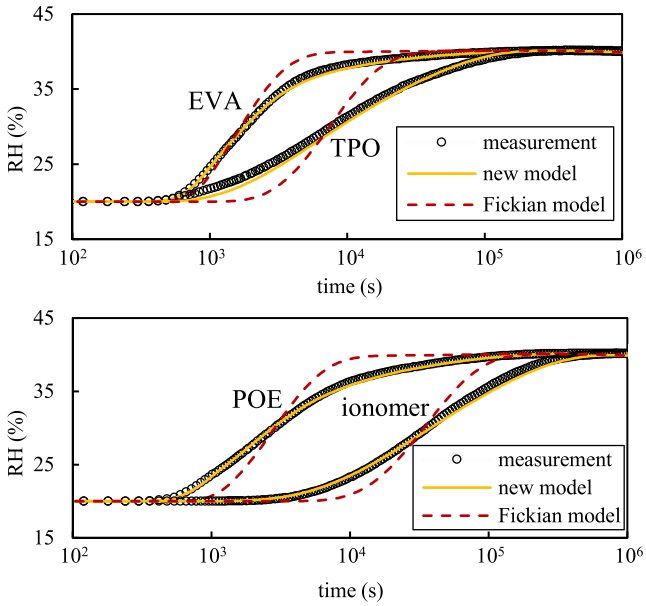

Fig. 14. Comparison between measurements and simulations with the new dual-transport model and the Fickian model. The top graph shows the results for EVA and TPO, the bottom for POE and ionomer.

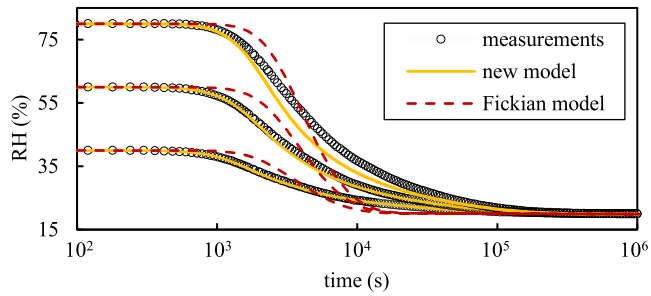

Fig. 15. Measured and simulated egress in POE.

linearity of the moisture ingress process. Optimized Fickian simulations in a homogeneous material (dashed lines) are added for comparison.

The measured ingress curves can vary between the three sensors in the same material. These differences are most pronounced in ionomer. The simulations with the corresponding thickness show that these differences are caused by the varying thickness of the encapsulant above the sensor.

The obtained parameters are used to simulate the egress from 80%, 60%, and 40% to 20% RH, respectively. The simulations yield good results for the latter, with a maximal absolute error of less than 1% RH in all encapsulants. However, the fit is worse for step changes with higher initial water concentrations. The dual-transport model overestimates the egress speed, resulting in an absolute error of up to 6.5% RH at 80% initial RH, as shown at the example of POE in Fig. 15. The maximal absolute error is around 2.5% with 60% initial RH. However, the model is still more accurate than the Fickian model, as shown in Fig. 15.

By changing the material parameters for egress, this issue can be resolved. A variation of D_C while keeping the other

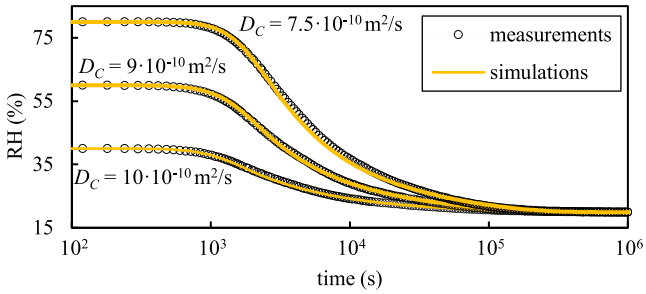

Fig. 16. Measured and simulated egress in POE using different values of parameter D_C that provide best fit in every case.

parameters constant is enough, as shown at the same example of POE in Fig. 16. The parameter D_C is 10 for the simulation of egress from 40% RH, 9 for the simulation of egress from 60% RH, and 7.5 in the simulation of egress from 80%.

VI. Discussion

The presented moisture transport model should be taken as a purely mathematical model for finite-element simulations. Nevertheless, its basic ideas and implementations have some foundation in the physical models of the diffusion processes in polymers, as described in the literature. However, the proposed mechanisms are applied to different polymeric materials. Until now, no models based on two transport mechanisms are applied specifically to PV encapsulants, making their direct application questionable and subject to further research. Nevertheless, we find two of them in line with the assumptions and their implementation into the model.

First is the free volume theory [29]. The channels are equivalent to the free volume, whereas the bulk is equivalent with the polymer matrix of the material. Positron lifetime spectroscopy measurements for EVA show that the fractional free volume is about 10% of the material, varying a few percent depending on the vinyl acetate (VA) and polyethylene (PE) contents [39]. POEs are usually ethylene-acrylate copolymers, which are suspected to behave similar to EVA. TPOs are commonly based on PE, suspected to be linear low density or low-density PE. Linear low-density PE measurements have shown a free volume in the range of 2%–4% [40]. However, to the best of our knowledge, no similar measurements of these encapsulants themselves and of ionomer are available in the literature.

The heterogeneity of the polymers is another possible explanation [25]. In PV EVA, usually around 30% of the material consists of the polar VA, whereas the majority is the nonpolar PE. EVA with a larger share of VA has shown to increase the overall diffusion coefficient of the material within certain limits [41], [42], indicating that on one hand the polarity leads to a faster diffusion. However, on the other hand, also the semicrystallinity of the material has to be considered. Crystalline zones are impermeable. The VA content in EVA reduces the degree of crystallinity, increasing the speed of diffusion through the material [43].

VII. Conclusion

The model presented in this article implements two transport mechanisms by proposing channels with higher diffusion coefficient through the bulk material and links it to measured macroscopic diffusion through the material. Even though the moisture flow in channels, bulk and across the interface is modeled as a Fickian diffusion process, we can accurately describe the observed non-Fickian diffusion cases. In these cases, diffusion through the material to an encapsulated sensor is primarily driven by the channels, whereas the bulk represents a hindering factor. Nevertheless, the model can describe simple Fickian diffusion cases as well.

The root mean square deviation (RMSD) between simulations and measurements is reduced by a factor between 3 and 10 using the new model instead of the homogeneous Fickian diffusion model, depending on the material and the boundary conditions. For example, the RMSD in TPO improves from 2.19% RH to 0.57% RH for the ingress simulations from 20% to 40%, shown in Fig. 14.

The model enables the prediction of moisture ingress after parameter optimization to a single measured ingress curve. Three parameters have to be determined. The share of channels S_C influences the interaction between the two regions and the amount of flow in both. The diffusion coefficient in the channels describes the speed of the diffusion process. The dimensionless parameter α, the ratio between the diffusion coefficients in channel and bulk, describes variations from the homogeneous Fickian model. It is purely a mathematical parameter, and not directly linked to any physical property of the material itself. As such, the bulk could be interpreted not only as a representation of a second process, but as a simple simulation equivalent of multiple processes affecting the diffusion in the material.

The same parameters result in a more accurate prediction than the Fickian model for ingress and egress at all measured RH ranges. However, the measurements show some nonlinear behavior in all four analyzed encapsulant materials at egress with high moisture concentration. The diffusion seems to exhibit some dependence on the moisture concentration, resulting in a hysteresis effect for ingress and egress at high RH.

Acknowledgment

The authors would like to thank D. Moser, EURAC Research, Bolzano, for useful discussion and laboratory access.

References

[1] D. L. King, M. A. Quintana, J. A. Kratochvil, D. E. Ellibee, and B. R. Hansen, "Photovoltaic module performance and durability following long-term field exposure," *Prog. Photovolt. Res. Appl.*, vol. 8, no. 2, pp. 241–256, Mar. 2000.

[2] IEA PVPS Task 13, *Review of Failures of Photovoltaic Modules,* International Energy Agency, Paris, France, Task 13, 2014.

[3] IEA PVPS Task 13, *Assessment of Photovoltaic Module Failures in the Field*, International Energy Agency, Paris, France, Task 13, 2017.

[4] A. W. Czanderna and F. J. Pern, "Encapsulation of PV modules using ethylene vinyl acetate copolymer as a pottant: A critical review," *Sol. Energy Mater. Sol. Cells*, vol. 43, no. 2, pp. 101–181, Sep. 1996.

[5] S. Hoffmann and M. Koehl, "Effect of humidity and temperature on the potential-induced degradation," *Prog. Photovolt. Res. Appl.*, vol. 22, no. 2, pp. 173–179, Feb. 2014.

[6] A. Fick, "Ueber diffusion," *Ann. Phys. Chem.*, vol. 170, no. 1, pp. 59–86, 1855.

[7] M. Kempe, "Modeling of rates of moisture ingress into photovoltaic modules," *Sol. Energy Mater. Sol. Cells*, vol. 90, no. 16, pp. 2720–2738, Oct. 2006.

[8] D. J. Coyle, "Life prediction for CIGS solar modules part 1: Modeling moisture ingress and degradation: Modeling moisture ingress and degradation," *Prog. Photovolt. Res. Appl.*, vol. 21, no. 2, pp. 156–172, Mar. 2013.

[9] P. Hülsmann, M. Heck, and M. Köhl, "Simulation of water vapor ingress into PV-modules under different climatic conditions," *J. Mater.*, vol. 2013, pp. 1–7, Feb. 2013.

[10] N. Kim and C. Han, "Experimental characterization and simulation of water vapor diffusion through various encapsulants used in PV modules," *Sol. Energy Mater. Sol. Cells*, vol. 116, pp. 68–75, Sep. 2013.

[11] M. D. Kempe, A. A. Dameron, and M. O. Reese, "Evaluation of moisture ingress from the perimeter of photovoltaic modules: Evaluation of moisture ingress," *Prog. Photovolt. Res. Appl.*, vol. 22, no. 11, pp. 1159–1171, Nov. 2014.

[12] P. Hülsmann and K.-A. Weiss, "Simulation of water ingress into PV-modules: IEC-testing versus outdoor exposure," *Sol. Energy*, vol. 115, pp. 347–353, May 2015.

[13] D. Wisniewski *et al.*, "Measurement and modelling of water ingress into double-glass photovoltaic modules," *Prog. Photovolt. Res. Appl.*, vol. 27, no. 2, pp. 144–151, Feb. 2019.

[14] A. Dadaniya and N. V. Datla, "Water diffusion simulation in photovoltaic module based on the characterization of encapsulant material using in-situ gravimetric technique," *Sol. Energy Mater. Sol. Cells*, vol. 201, Oct. 2019, Art. no. 110063.

[15] J. Slapsak, S. Mitterhofer, M. Topic, and M. Jankovec, "Wireless system for *In Situ* monitoring of moisture ingress in PV modules," *IEEE J. Photovolt.*, vol. 9, no. 5, pp. 1316–1323, Sep. 2019.

[16] Y. Diamant, G. Marom, and L. J. Broutman, "The effect of network structure on moisture absorption of epoxy resins," *J. Appl. Polym. Sci.*, vol. 26, no. 9, pp. 3015–3025, Sep. 1981.

[17] P. Neogi, "A hole-filling theory of anomalous diffusion in glassy polymers. Effects of microvoids," *J. Polym. Sci. Part B, Polym. Phys.*, vol. 31, no. 6, pp. 699–710, May 1993.

[18] J. Sharma, K. Tewari, and R. K. Arya, "Diffusion in polymeric systems—A review on free volume theory," *Prog. Org. Coat.*, vol. 111, pp. 83–92, Oct. 2017.

[19] M. Hedenqvist, "Diffusion of small-molecule penetrants in semicrystalline polymers," *Prog. Polym. Sci.*, vol. 21, no. 2, pp. 299–333, 1996.

[20] E. E. Shafee and H. F. Naguib, "Water sorption in cross-linked poly(vinyl alcohol) networks," *Polymer*, vol. 44, no. 5, pp. 1647–1653, Mar. 2003.

[21] G. Yaniv and O. Ishai, "Coupling between stresses and moisture diffusion in polymeric adhesives," *Polym. Eng. Sci.*, vol. 27, no. 10, pp. 731–739, May 1987.

[22] D. A. Bond and P. A. Smith, "Modeling the transport of low-molecular-weight penetrants within polymer matrix composites," *Appl. Mech. Rev.*, vol. 59, no. 5, p. 249, 2006.

[23] Y. Weitsman, "Coupled damage and moisture-transport in fiber-reinforced, polymeric composites," *Int. J. Solids Struct.*, vol. 23, no. 7, pp. 1003–1025, 1987.

[24] S. Mitterhofer, M. Jankovec, and M. Topic, "One- and two-dimensional finite element analysis of humidity ingress in polymeric materials," in *Proc. 54th Int. Conf. Microelectron., Devices Mater.*, Ljubljana, Slovenia, 2018, pp. 93–98.

[25] C. Maggana and P. Pissis, "Water sorption and diffusion studies in an epoxy resin system," *J. Polym. Sci. B Polym. Phys.*, vol. 37, no. 11, pp. 1165–1182, Jun. 1999.

[26] P. M. Jacobs and F. R. Jones, "Diffusion of moisture into two-phase polymers: Part 1 - The development of an analytical model and its application to styrene-ethylenelbutylene-styrene block copolymer," *J. Mater. Sci.*, vol. 24, no. 7, pp. 2331–2336, Jul. 1989.

[27] S. Popineau, C. Rondeau-Mouro, C. Sulpice-Gaillet, and M. E. R. Shanahan, "Free/bound water absorption in an epoxy adhesive," *Polymer*, vol. 46, no. 24, pp. 10733–10740, Nov. 2005.

[28] J. Zhou and J. P. Lucas, "Hygrothermal effects of epoxy resin. Part I: The nature of water in epoxy," *Polymer*, vol. 40, no. 20, pp. 5505–5512, Sep. 1999.

[29] M. Y. M. Chiang and M. Fernandez-Garcia, "Relation of swelling and Tg depression to the apparent free volume of a particle-filled, epoxy-based adhesive," *J. Appl. Polym. Sci.*, vol. 87, no. 9, pp. 1436–1444, Feb. 2003.

[30] J. S. Vrentas, J. L. Duda, and A.-C. Hou, "Anomalous sorption in poly(ethyl methacrylate)," *J. Appl. Polym. Sci.*, vol. 29, no. 1, pp. 399–406, Jan. 1984.

[31] H. G. Carter and K. G. Kibler, "Langmuir-type model for anomalous moisture diffusion in composite resins," *J. Compos. Mater.*, vol. 12, no. 2, pp. 118–131, Jul. 1978.
[32] M. D. Placette, X. Fan, J.-H. Zhao, and D. Edwards, "A dual stage model of anomalous moisture diffusion and desorption in epoxy mold compounds," in *Proc. 12th Int. Conf. Thermal, Mech. Multi-Phys. Simul. Exp. Microelectron. Microsyst.*, Linz, Austria, 2011, pp. 1–8.
[33] W. Lei, M. K. Rigozzi, and D. R. McKenzie, "The physics of confined flow and its application to water leaks, water permeation and water nanoflows: A review," *Rep. Prog. Phys.*, vol. 79, no. 2, Feb. 2016, Art. no. 25901.
[34] M. Jankovec *et al.*, "*In-Situ* monitoring of moisture ingress in PV modules using digital humidity sensors," *IEEE J. Photovolt.*, vol. 6, no. 5, pp. 1152–1159, Sep. 2016.
[35] M. Jankovec, E. Annigoni, C. Ballif, and M. Topic, "In-situ determination of moisture diffusion properties of pv module encapsulants using digital humidity sensors," in *Proc. IEEE 7th World Conf. Photovol. Energy Convers.*, Waikoloa Village, HI, USA, 2018, pp. 415–417.
[36] F. Hecht, "New development in freefem++," *J. Numer. Math.*, vol. 20, no. 3–4, Jan. 2012.
[37] J. Crank and P. Nicolson, "A practical method for numerical evaluation of solutions of partial differential equations of the heat-conduction type," *Adv. Comput. Math.*, vol. 6, no. 1, pp. 207–226, Dec. 1996.
[38] M. Jankovec *et al.*, "Long term stability of humidity sensors, laminated in EVA encapsulant," presented at the 51st Int. Conf. Microelectron., Devices Mater., Bled, Slovenia, 2015.
[39] G. Dlubek, T. Lüpke, J. Stejny, M. A. Alam, and M. Arnold, "Local free volume in ethylene−vinyl acetate copolymers: A positron lifetime study," *Macromolecules*, vol. 33, no. 3, pp. 990–996, Feb. 2000.
[40] M. A. Sweed, "Free volume properties of semi-crystalline polymers," Ph.D. dissertation, Univ. Stellenbosch, Stellenbosch, South Africa, 2011.
[41] S. Marais, Q. T. Nguyen, D. Langevin, and M. Métayer, "Transport of water and gases through EVA copolymer films, EVA70/PVC, and EVA70/PVC/gluten blends," *Macromol. Symp.*, vol. 175, no. 1, pp. 329–348, Oct. 2001.
[42] S. Marais *et al.*, "Permeation and sorption of water and gases through EVA copolymers films," *Mater. Res. Innov.*, vol. 6, no. 2, pp. 79–88, Sep. 2002.
[43] C. Hirschl *et al.*, "Determining the degree of crosslinking of ethylene vinyl acetate photovoltaic module encapsulants—A comparative study," *Sol. Energy Mater. Sol. Cells*, vol. 116, pp. 203–218, Sep. 2013.